Microscopic optical potentials for ^{4}He scattering

Kei Egashira,[1,*] Kosho Minomo,[2,†] Masakazu Toyokawa,[1,‡] Takuma Matsumoto,[1,§] and Masanobu Yahiro[1,‖]
[1]*Department of Physics, Kyushu University, Fukuoka 812-8581, Japan*
[2]*Research Center for Nuclear Physics, Osaka University, Ibaraki 567-0047, Japan*
(Received 3 April 2014; published 26 June 2014)

We present a reliable double-folding (DF) model for ^{4}He-nucleus scattering, using the Melbourne g-matrix nucleon-nucleon interaction that explains nucleon-nucleus scattering with no adjustable parameter. In the DF model, only the target density is taken as the local density in the Melbourne g matrix. For ^{4}He elastic scattering from ^{58}Ni and ^{208}Pb targets in a wide range of incident energies from 20 to 200 MeV/nucleon, the DF model with the target-density approximation (TDA) yields much better agreement with the experimental data than the usual DF model with the frozen-density approximation in which the sum of projectile and target densities is taken as the local density. We also discuss the relation between the DF model with the TDA and the conventional folding model in which the nucleon-nucleus potential is folded with the ^{4}He density.

DOI: 10.1103/PhysRevC.89.064611 PACS number(s): 25.55.Ci, 24.10.Ht

I. INTRODUCTION

Microscopic derivation of nucleon-nucleus (NA) and nucleus-nucleus (AA) optical potentials is a goal of nuclear reaction theory. The optical potential is an important quantity to describe not only elastic scattering but also more complicated reactions such as inelastic scattering, breakup, and transfer reactions. For the latter case, the optical potential is used as a key input in theoretical calculations such as the distorted-wave Born approximation (DWBA) and the continuum discretized coupled-channels (CDCC) method [1–3].

The g-matrix folding model is a powerful tool for deriving NA and AA optical potentials. In the model, the optical potential is calculated by folding the g-matrix effective nucleon-nucleon (NN) interaction [4–13] with the target density for NA scattering and the projectile and target densities for AA scattering; see, for example, Refs. [14–18] for the folding procedure. The folding model for NA and AA scattering are referred to as the single-folding model and the double-folding (DF) model, respectively. For NA elastic scattering, the model is quite successful in reproducing the experimental data systematically with no free parameter, when the Melbourne g matrix [11] is used as an effective NN interaction in the folding calculations. As an important advantage of the g-matrix folding model, the model takes account of nuclear medium effects. The g matrix is calculated in nuclear matter and hence depends on nuclear-matter density ρ. When the optical potential is evaluated from the g matrix in the folding procedure, the nuclear-matter density is replaced by the target density at the location of the interacting nucleon pair. This approximation is called the local-density approximation.

The NA potential thus derived is nonlocal and thereby not so practical in many applications. It is, however, possible to localize the potential with the Brieva-Rook approximation [6]. Recently, the validity of the approximation was shown in Refs. [19,20]. In fact, the local version of the g-matrix folding potential describes NA scattering with no adjustable parameter [21] and is close to the phenomenological NA optical potentials [22–25].

From a theoretical viewpoint based on multiple scattering theory [26–28], the multiple NN scattering series in an AA collision [28] is more complicated than that in an NA collision [26,27]. In this sense, a microscopic understanding of the optical potentials is relatively more difficult for AA scattering than for NA scattering. One of the simplest composite projectiles is ^{4}He, since it is almost inert. For ^{4}He-nucleus elastic scattering, a systematic analysis was made [29] by using the g-matrix interaction proposed by Jeukenne, Lejeune, and Mahaux (JLM) [5]. The JLM g-matrix folding model reproduces measured differential cross sections for ^{4}He elastic scattering at incident energies ranging from 10 to 60 MeV/nucleon, if the real and imaginary parts of the folding potential are reduced by about 25% and 35%, respectively. In the JLM g matrix, nuclear medium effects are included only partly, so that normalization factors are always introduced. This fact strongly suggests that a parameter-free analysis based on the Melbourne g-matrix folding model should be made for ^{4}He-nucleus elastic scattering.

In the DF procedure, the frozen-density approximation (FDA) is usually taken. Namely, one takes as the local density the sum of projectile and target densities, $\rho_{\rm P}$ and $\rho_{\rm T}$, at the midpoint of the two interacting nucleons, one in the projectile (P) and the other in the target (T):

$$g(\rho) = g(\rho_{\rm P} + \rho_{\rm T}). \tag{1}$$

Very recently, the Melbourne g-matrix folding model with the FDA was applied to ^{12}C + ^{12}C and $^{20-32}$Ne + ^{12}C elastic scattering at intermediate energies with success in reproducing measured differential cross sections $d\sigma/d\Omega$ and total reaction cross sections $\sigma_{\rm R}$ with no free parameter [18,30,31]. In the calculations, the densities of unstable nuclei $^{20-32}$Ne were evaluated by antisymmetrized molecular dynamics (AMD) [32,33] with the Gogny-D1S interaction [34]. The AMD wave functions successfully describe low-lying spectra

*egashira@phys.kyushu-u.ac.jp
†minomo@rcnp.osaka-u.ac.jp
‡toyokawa@phys.kyushu-u.ac.jp
§matsumoto@phys.kyushu-u.ac.jp
‖yahiro@phys.kyushu-u.ac.jp

of Ne isotopes [32]. The microscopic approach concluded that $^{30-32}$Ne in the "island of inversion" have large deformation and ^{31}Ne has a deformed halo structure [18,30,31]. This indicates that the $N = 20$ magicity disappears. The Melbourne g-matrix folding model is thus a powerful tool for not only understanding the reaction mechanism but also determining the structure of unstable nuclei.

In this paper, we microscopically describe ^{4}He elastic scattering from heavier targets such as ^{58}Ni and ^{208}Pb in a wide range of incident energies from 20 to 200 MeV/nucleon, using the Melbourne g-matrix DF model with no adjustable parameter. After showing that the DF model with the FDA cannot reproduce measured $d\sigma/d\Omega$ and $\sigma_{\rm R}$ for the scattering, we propose a new approximation instead of the FDA. In the approximation, only the target density is taken as the local density. This approximation is referred to as the target-density approximation (TDA) in this paper. The reliability of the TDA is shown theoretically by using multiple scattering theory [26–28] and phenomenologically by showing that the DF model with the TDA well reproduces the data on $d\sigma/d\Omega$ and $\sigma_{\rm R}$. We also investigate the reliability of the conventional nucleon-nucleus folding (NAF) model in which the NA potential is folded with the ^{4}He density.

In Sec. II, we recapitulate the Melbourne g-matrix DF model and show the reliability of the TDA theoretically. Numerical results are shown in Sec. III. Section IV is devoted to a summary.

II. MODEL BUILDING

AA scattering can be described by the many-body Schrödinger equation,

$$\left(T_R + h_{\rm P} + h_{\rm T} + \sum_{i\in{\rm P}, j\in{\rm T}} v_{ij} - E\right)\Psi^{(+)} = 0, \tag{2}$$

with the realistic NN interaction v_{ij}, where T_R stands for the kinetic energy with respect to the relative coordinate ($\boldsymbol{R}$) between the projectile (P) and the target (T), E is the total energy, and $h_{\rm P}$ ($h_{\rm T}$) means the internal Hamiltonian of P (T). Using multiple scattering theory [26,27] for AA scattering [28], one can rewrite Eq. (2) as

$$\left(T_R + h_{\rm P} + h_{\rm T} + \sum_{i\in{\rm P}, j\in{\rm T}} \tau_{ij} - E\right)\hat{\Psi}^{(+)} = 0 \tag{3}$$

with the effective NN interaction τ_{ij} defined by

$$\tau_{ij} = v_{ij} + v_{ij}G_0\tau_{ij} \tag{4}$$

with

$$G_0 = \frac{\mathcal{P}_{\rm P}\mathcal{P}_{\rm T}}{E - T_R - h_{\rm P} - h_{\rm T} + i\epsilon}, \tag{5}$$

where $\mathcal{P}_{\rm P}$ ($\mathcal{P}_{\rm T}$) denotes the projection operator onto the space of antisymmetrized wave functions of P (T). In the derivation of Eq. (3), the antisymmetrization between nucleons in P and those in T has been neglected, but it is shown in Refs. [36,37] that antisymmetrization effects are well taken care of by using a τ_{ij} that is properly symmetrical with respect to the exchange of colliding nucleons. Since the effective NN interaction τ_{ij} includes nuclear medium effects, the g matrix (g_{ij}) is often used as such a τ_{ij} [4–12,16].

Since g_{ij} includes projectile- and target-excitation effects approximately, Eq. (3) can be further rewritten into the single-channel equation

$$[T_R + U - E_{\rm in}]\psi = 0, \tag{6}$$

with the folding potential

$$U(\boldsymbol{R}) = \langle\Phi_0| \sum_{i\in{\rm P}, j\in{\rm T}} g_{ij}|\Phi_0\rangle, \tag{7}$$

where the incident energy $E_{\rm in}$ is related to the total energy E as $E = E_{\rm in} + e_0({\rm P}) + e_0({\rm T})$ for the ground-state energies, e_0(P) and e_0(T), of P and T. The wave function Φ_0 denotes the product of the ground states of P and T, while ψ means the relative wave function between P and T. This is nothing but the g-matrix DF model. In the actual calculations, the FDA shown in Eq. (1) is usually taken and the Coulomb potential $U_{\rm Coul}$ is added to the resulting U.

The folding potential is a key quantity to describe not only elastic scattering but also other direct reactions. Inelastic scattering to noncollective excited states and transfer reactions are analyzed with the DWBA, whereas breakup reactions are investigated the using CDCC method. The folding potential is an essential input of the DWBA and CDCC calculations. For inelastic scattering to states excited by vibrational and rotational modes, we can consider two methods: the DWBA and the coupled-channel formalism in which coupling potentials among elastic and inelastic channels are obtained by folding g_{ij} with the corresponding transition densities of P and T [35]. At the present stage, it is not clear which method is more reasonable, since the g_{ij} includes projectile- and target-excitation effects on the elastic channel approximately. This is an interesting question to be clarified in future.

Now we consider ^{4}He scattering from heavier nuclei. In the scattering, the projectile (^{4}He) is hardly excited, whereas the target is excited easily. As a good approximation we can hence neglect projectile excitations. Namely, we can replace $h_{\rm P}$ by the ground-state energy e_0(P) and hence $\mathcal{P}_{\rm P}\mathcal{P}_{\rm T}$ by $\mathcal{P}_{\rm T}$:

$$G_0 \approx \frac{\mathcal{P}_{\rm T}}{E - T_R - e_0({\rm P}) - h_{\rm T} + i\epsilon}. \tag{8}$$

After the approximation, the τ_{ij} includes nuclear medium effects from T, but not from P. We should therefore replace τ_{ij} by the g matrix depending only on $\rho_{\rm T}$:

$$g(\rho) = g(\rho_{\rm T}). \tag{9}$$

This is the TDA proposed in the present paper. The reliability of the TDA is confirmed also phenomenologically in Sec. III by comparing the theoretical results with the experimental data and showing that the TDA is much better than the FDA.

Next we recapitulate the single-folding model for NA scattering and the DF model for AA scattering. For detail of the models, for example, see Refs. [6,12,13,15,19,21] for NA scattering and Refs. [12,14,17,18,20] for AA scattering. The DF potential $U = V + iW$ consists of the direct and exchange parts, $U^{\rm DR}$ and $U^{\rm EX}$ [14,17]:

$$U(\boldsymbol{R}) = U^{\rm DR}(\boldsymbol{R}) + U^{\rm EX}(\boldsymbol{R}) + U_{\rm Coul}(\boldsymbol{R}) \tag{10}$$

with

$$U^{\rm DR}(\boldsymbol{R}) = \sum_{\mu,\nu}\int \rho_{\rm P}^{\mu}(\boldsymbol{r}_{\rm P})\rho_{\rm T}^{\nu}(\boldsymbol{r}_{\rm T})g_{\mu\nu}^{\rm DR}(s;\rho_{\mu\nu})d\boldsymbol{r}_{\rm P}d\boldsymbol{r}_{\rm T}, \quad (11)$$

$$U^{\rm EX}(\boldsymbol{R}) = \sum_{\mu,\nu}\int \tilde{\rho}_{\rm P}^{\mu}(\boldsymbol{r}_{\rm P},\boldsymbol{r}_{\rm P}-\boldsymbol{s})\tilde{\rho}_{\rm T}^{\nu}(\boldsymbol{r}_{\rm T},\boldsymbol{r}_{\rm T}+\boldsymbol{s}) \times g_{\mu\nu}^{\rm EX}(s;\rho_{\mu\nu})\exp\left[-i\boldsymbol{K}(\boldsymbol{R})\cdot\boldsymbol{s}/M\right]d\boldsymbol{r}_{\rm P}d\boldsymbol{r}_{\rm T}, \quad (12)$$

where $\boldsymbol{r}_{\rm P}$ ($\boldsymbol{r}_{\rm T}$) stands for the coordinate of the interacting nucleon from the center of mass of P (T), $\boldsymbol{s} = \boldsymbol{r}_{\rm P} - \boldsymbol{r}_{\rm T} + \boldsymbol{R}$, and each of μ and ν denotes the z component of isospin. Here the one-body and mixed densities, $\rho_{\rm P}^{\mu}(\boldsymbol{r}_{\rm P})$ and $\tilde{\rho}_{\rm P}^{\mu}(\boldsymbol{r}_{\rm P},\boldsymbol{r}_{\rm P}-\boldsymbol{s})$, of P are defined by

$$\rho_{\rm P}^{\mu}(\boldsymbol{r}_{\rm P}) = \sum_{a}\phi_{{\rm P};a}^{*\mu}(\boldsymbol{r}_{\rm P})\phi_{{\rm P};a}^{\mu}(\boldsymbol{r}_{\rm P}), \quad (13)$$

$$\tilde{\rho}_{\rm P}^{\mu}(\boldsymbol{r}_{\rm P},\boldsymbol{r}_{\rm P}-\boldsymbol{s}) = \sum_{a}\phi_{{\rm P};a}^{*\mu}(\boldsymbol{r}_{\rm P})\phi_{{\rm P};a}^{\mu}(\boldsymbol{r}_{\rm P}-\boldsymbol{s}) \quad (14)$$

with the single-particle wave function $\phi_{{\rm P};a}(\boldsymbol{r}_{\rm P})$ of P classified with the quantum number a. The one-body and mixed densities, $\rho_{\rm T}^{\mu}(\boldsymbol{r}_{\rm T})$ and $\tilde{\rho}_{\rm T}^{\mu}(\boldsymbol{r}_{\rm T},\boldsymbol{r}_{\rm T}+\boldsymbol{s})$, of T are defined in the same way.

The nonlocal $U^{\rm EX}$ has been localized in Eq. (12) with the local semiclassical approximation [6], where the local momentum $\hbar\boldsymbol{K}(\boldsymbol{R})$ of P relative to T is defined by $\hbar K(R) \equiv \sqrt{2\mu_{\rm PT}[E_{\rm in} - U(R)]}$ with the reduced mass $\mu_{\rm PT}$ between P and T, and $M = A_{\rm P}A_{\rm T}/(A_{\rm P}+A_{\rm T})$ for the mass numbers, $A_{\rm P}$ and $A_{\rm T}$, of P and T. The validity of the localization is shown in Refs. [19,20]. The direct and exchange parts, $g_{\mu\nu}^{\rm DR}$ and $g_{\mu\nu}^{\rm EX}$, of the g matrix depend on the local density at the midpoint of the interacting nucleon pair:

$$\rho_{\mu\nu} = \rho_{\rm P}^{\mu}(\boldsymbol{r}_{\rm P}-\boldsymbol{s}/2) + \rho_{\rm T}^{\nu}(\boldsymbol{r}_{\rm T}+\boldsymbol{s}/2) \quad (15)$$

in the FDA and

$$\rho_{\mu\nu} = \rho_{\rm T}^{\nu}(\boldsymbol{r}_{\rm T}+\boldsymbol{s}/2) \quad (16)$$

in the TDA; see Ref. [18] for the explicit forms of $g_{\mu\nu}^{\rm DR}$ and $g_{\mu\nu}^{\rm EX}$. In Eqs. (11) and (12), the folding potentials are calculated by direct numerical integration in the coordinate space.

We now consider NA scattering at an incident energy $E_{\rm in}^{\rm N}$. The single-folding potentials $U_\mu = V_\mu + iW_\mu$ for proton ($\mu = -1/2$) and neutron ($\mu = 1/2$) scattering are also composed of $U_\mu^{\rm DR}$ and $U_\mu^{\rm EX}$:

$$U_\mu(\boldsymbol{r}_\mu) = U_\mu^{\rm DR}(\boldsymbol{r}_\mu) + U_\mu^{\rm EX}(\boldsymbol{r}_\mu) + U_{\rm Coul}(\boldsymbol{r}_\mu) \quad (17)$$

with

$$U_\mu^{\rm DR}(\boldsymbol{r}_\mu) = \sum_{\nu}\int \rho_{\rm T}^{\nu}(\boldsymbol{r}_{\rm T})g_{\mu\nu}^{\rm DR}(s;\rho_{\mu\nu})d\boldsymbol{r}_{\rm T}, \quad (18)$$

$$U_\mu^{\rm EX}(\boldsymbol{r}_\mu) = \sum_{\nu}\int \tilde{\rho}_{\rm T}^{\nu}(\boldsymbol{r}_{\rm T},\boldsymbol{r}_{\rm T}+\boldsymbol{s}) \times g_{\mu\nu}^{\rm EX}(s;\rho_{\mu\nu})\exp\left[-i\boldsymbol{K}_\mu(\boldsymbol{r}_\mu)\cdot\boldsymbol{s}\right]d\boldsymbol{r}_{\rm T}, \quad (19)$$

where $\boldsymbol{s} = \boldsymbol{r}_\mu - \boldsymbol{r}_{\rm T}$ with $\boldsymbol{r}_\mu$ the coordinate of an incident nucleon from the center of mass of T, the local density $\rho_{\mu\nu}$ is obtained by Eq. (16), and the local momentum $\hbar\boldsymbol{K}_\mu(\boldsymbol{r}_\mu)$ between the incident nucleon (N) and T is defined by $\hbar K_\mu(r_\mu) \equiv \sqrt{2\mu_{\rm NT}[E_{\rm in}^{\rm N} - U_\mu(r_\mu)]}$ for the reduced mass $\mu_{\rm NT}$ between N and T.

When AA scattering at high $E_{\rm in}$ is compared with NA scattering at $E_{\rm in}^{\rm N} = E_{\rm in}/A_{\rm P}$ for heavy targets satisfying $A_{\rm T} \gg A_{\rm P} > 1$, the local momenta $\hbar\boldsymbol{K}_\mu(\boldsymbol{r}_\mu)$ and $\hbar\boldsymbol{K}(\boldsymbol{R})$ nearly agree with their asymptotic values $\hbar\boldsymbol{K}_\mu(\infty)$ and $\hbar\boldsymbol{K}(\infty)$, respectively, that satisfy the relation

$$\boldsymbol{K}_\mu(\infty) = \boldsymbol{K}(\infty)/M. \quad (20)$$

Taking the relation (20) and the TDA, one can get

$$U^{\rm DR}(\boldsymbol{R}) \approx \sum_{\mu}\int \rho_{\rm P}^{\mu}(\boldsymbol{r}_{\rm P})U_\mu^{\rm DR}(\boldsymbol{R}+\boldsymbol{r}_{\rm P})d\boldsymbol{r}_{\rm P}, \quad (21)$$

$$U^{\rm EX}(\boldsymbol{R}) \approx \sum_{\mu}\int \rho_{\rm P}^{\mu}(\boldsymbol{r}_{\rm P})U_\mu^{\rm EX}(\boldsymbol{R}+\boldsymbol{r}_{\rm P})d\boldsymbol{r}_{\rm P}. \quad (22)$$

In the derivation of Eq. (22), we have also used the approximation $\tilde{\rho}_{\rm P}^{\mu}(\boldsymbol{r}_{\rm P},\boldsymbol{r}_{\rm P}-\boldsymbol{s}) \approx \tilde{\rho}_{\rm P}^{\mu}(\boldsymbol{r}_{\rm P},\boldsymbol{r}_{\rm P}) = \rho_{\rm P}^{\mu}(\boldsymbol{r}_{\rm P})$, which if good in the peripheral region of T that is important for elastic scattering [19]. For ^{4}He scattering from heavier targets at high $E_{\rm in}$, the DF potential $U^{\rm DR} + U^{\rm EX}$ with the TDA is thus obtained with reasonable accuracy by folding the nucleon-nucleus potential $U_\mu^{\rm DR} + U_\mu^{\rm EX}$ with the projectile density $\rho_{\rm P}^{\mu}$. This is the NAF model mentioned in Sec. I. This model is quite practical, since one can use the phenomenological NA optical potential instead of U_μ. The validity of this model is also investigated later in Sec. III. The condition that the local momenta $\hbar\boldsymbol{K}_\mu(\boldsymbol{r}_\mu)$ and $\hbar\boldsymbol{K}(\boldsymbol{R})$ are close to their asymptotic values is well satisfied at large R, even if $E_{\rm in}$ is small. Since ^{4}He scattering from heavy targets is quite peripheral at small $E_{\rm in}$, one can expect that the NAF model is good also for small $E_{\rm in}$. This is also discussed in Sec. III.

III. RESULTS

We analyzed the measured $d\sigma/d\Omega$ and $\sigma_{\rm R}$ for ^{4}He elastic scattering from ^{58}Ni and ^{208}Pb targets in the region $20 \lesssim E_{\rm in}/A_{\rm P} \lesssim 200$ MeV, using the following three models:

(1) the DF model with the TDA (the DF-TDA model),
(2) the DF model with the FDA (the DF-FDA model), and
(3) the NAF model.

For the ^{4}He density $\rho_{\rm P}$, we use the phenomenological proton-density [38] determined from electron scattering in which the finite-size effect due to the proton charge is unfolded in the standard manner [39]. The neutron density is assumed to have the same geometry as the proton one. For the target density $\rho_{\rm T}$, we take the matter densities calculated by the spherical Hartree-Fock (HF) model with the Gogny-D1S interaction [34] in which the spurious center-of-mass motion is removed in the standard manner [18].

Figure 1 shows $d\sigma/d\Omega$ as a function of transfer momentum q for ^{4}He + ^{58}Ni scattering at $E_{\rm in}/A_{\rm P} = 20$–$175$ MeV. For lower incident energies of $E_{\rm in}/A_{\rm P} = 20$–$60$ MeV, the DF-FDA model (dotted line) overestimates the experimental data [40–43], but this problem is solved by the DF-TDA model

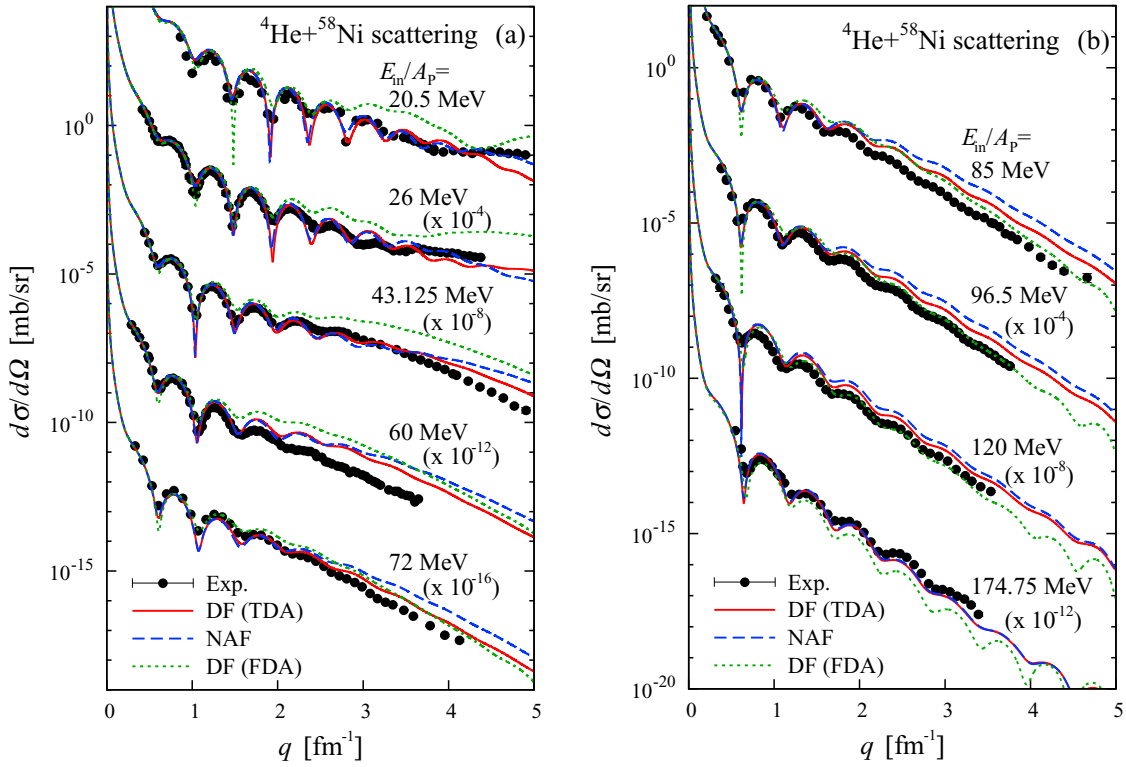

FIG. 1. (Color online) Differential cross sections as a function of transfer momentum q for ^{4}He + ^{58}Ni elastic scattering at (a) E_{in}/A_P = 20–72 MeV and (b) E_{in}/A_P = 85–175 MeV. The cross section at each E_{in}/A_P is multiplied by the factor shown in the panel. The solid (dotted) line stands the results of the DF-TDA (DF-FDA) model, whereas the dashed line denotes the results of the NAF model. The experimental data are taken from Refs. [40–45].

(solid line), which well reproduces the data. For higher energies around E_{in}/A_P = 175 MeV, meanwhile, the DF-FDA model underestimates the experimental data [44], but this problem is also solved by the DF-TDA model, which reproduces the data. For intermediate energies of E_{in}/A_P = 72–120 MeV, the difference between the DF-TDA and DF-FDA results is rather small, so both the models reasonably reproduce the data. In great detail, for E_{in}/A_P = 85 MeV, the DF-TDA result is better than the DF-FDA result at $q \lesssim 2$ fm^{-1}, whereas the latter is better than the former at $q \gtrsim 3$ fm^{-1}. For E_{in}/A_P = 97 MeV, the DF-FDA model is slightly better than the DF-TDA model,

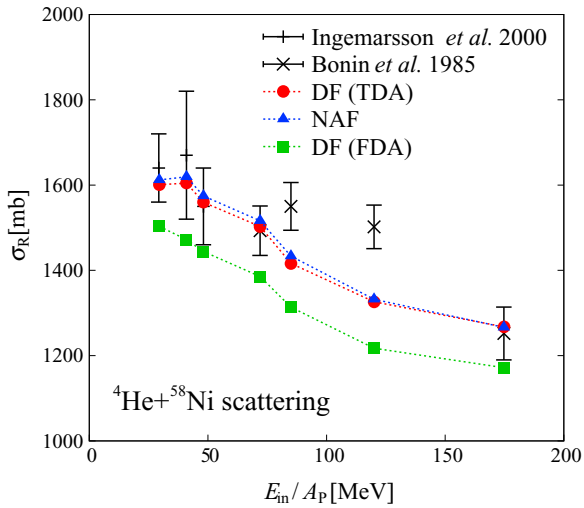

FIG. 2. (Color online) Total reaction cross section σ_R as a function of E_{in}/A_P for ^{4}He + ^{58}Ni scattering at E_{in}/A_P = 20–175 MeV. The circles (squares) stand the results of the DF-TDA (DF-FDA) model, whereas the triangles denote the results of the NAF model. The experimental data are taken from [44,46].

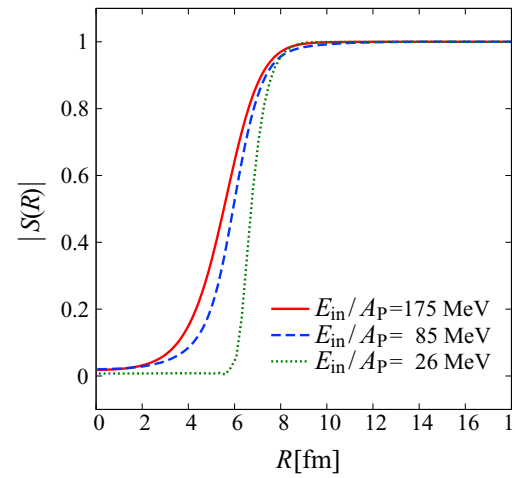

FIG. 3. (Color online) R dependence of the absolute value of the elastic S-matrix element for ^{4}He + ^{58}Ni elastic scattering at E_{in}/A_P = 26, 85, and 175 MeV. The solid, dashed, and dotted lines represent the elastic S-matrix elements calculated with the DF-TDA model at E_{in}/A_P = 26, 85, and 175 MeV, respectively.

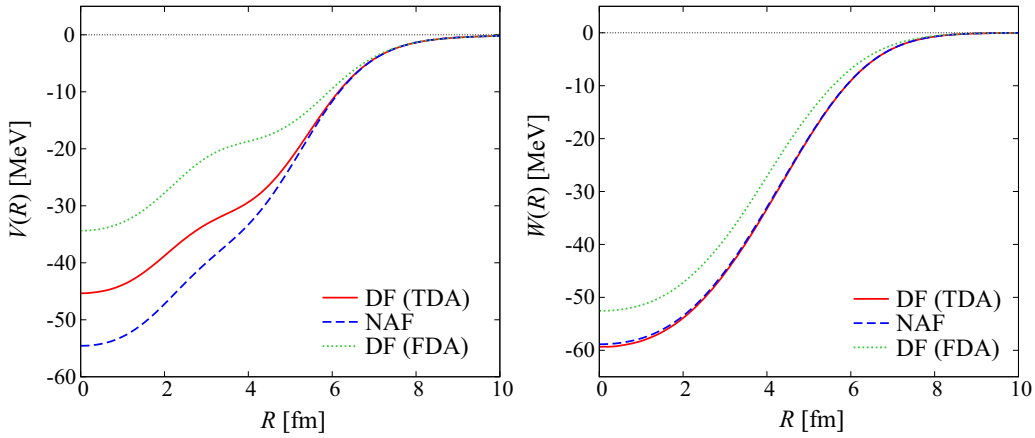

FIG. 4. (Color online) Optical potentials for ^{4}He + ^{58}Ni elastic scattering at $E_{\rm in}/A_{\rm P} = 175$ MeV. The solid (dotted) line stands for the DF-TDA (DF-FDA) potential, whereas the dashed line denotes the NAF potential.

but this seems to be accidental, since for $\sigma_{\rm R}$ the DF-TDA model (circles) yields better agreement with the data [44,46] than the DF-FDA model (squares), as shown in Fig. 2. From these analyses, we can conclude that the DF-TDA model is much better than the DF-FDA model.

Next we compare the DF-TDA model with the NAF model in Figs. 1 and 2. For $\sigma_{\rm R}$, the NAF model (triangles) well simulates the DF-TDA result (circles) and hence yields much better agreement with the data [44,46] than the DF-FDA model (squares). For $d\sigma/d\Omega$ at higher energies of $E_{\rm in}/A_{\rm P} =$ 120–175 MeV, as expected, the NAF results (dashed lines) well reproduce the DF-TDA results (solid lines). Also for lower energies of $E_{\rm in}/A_{\rm P} = 20$–43 MeV, the NAF model well simulates the DF-TDA results, since the elastic scattering is quite peripheral, as shown below. For intermediate energies of $E_{\rm in}/A_{\rm P} = 60$–97 MeV, however, the NAF results deviate sizably from the DF-TDA results.

Figure 3 shows the absolute value of the elastic S-matrix element as a function of R for ^{4}He + ^{58}Ni elastic scattering, where R is estimated from the angular momentum L between P and T with the semiclassical relation $L = RK(\infty)$. The solid, dashed, and dotted lines correspond to the elastic S-matrix elements calculated with the DF-TDA model at $E_{\rm in}/A_{\rm P} = 26$, 85, and 175 MeV, respectively. The ^{4}He scattering becomes more peripheral as $E_{\rm in}/A_{\rm P}$ decreases. Particularly at $E_{\rm in}/A_{\rm P} =$ 26 MeV, the scattering is quite peripheral. This is the reason why the NAF model well simulates the DF-TDA model for lower energies of $E_{\rm in}/A_{\rm P} = 20$–43 MeV. Eventually, the NAF model is good not only for higher energies of $E_{\rm in}/A_{\rm P} =$ 120–175 MeV but also for lower energies of $E_{\rm in}/A_{\rm P} =$ 20–43 MeV.

Figure 4 shows the folding potentials $U = V + iW$ for ^{4}He + ^{58}Ni elastic scattering at $E_{\rm in}/A_{\rm P} = 175$ MeV. The FDA has stronger Pauli-blocking effects than the TDA because of $\rho_{\rm P} + \rho_{\rm T} \geqslant \rho_{\rm P}$. As a result of this property, the DF-FDA potential (dotted line) is less attractive and less absorptive than the DF-TDA potential (solid line). The NAF model (dashed line) well simulates the DF-TDA potential in $R \gtrsim 5$ fm, as expected. This is the reason why at $E_{\rm in}/A_{\rm P} = 175$ MeV the NAF model well simulates the DF-TDA model for both $d\sigma/d\Omega$ and $\sigma_{\rm R}$.

Figures 5 and 6 show the folding potentials for ^{4}He + ^{58}Ni elastic scattering at $E_{\rm in}/A_{\rm P} = 85$ and 26 MeV, respectively. The Pauli-blocking effects due to $\rho_{\rm P}$, which is represented by the difference between the DF-TDA and DF-FDA potentials, become large as $E_{\rm in}/A_{\rm P}$ decreases, as expected. For $E_{\rm in}/A_{\rm P} =$ 26 MeV, the NAF potential reproduces the DF-TDA potential for $R \gtrsim 5$ fm, but the former largely deviates from the latter

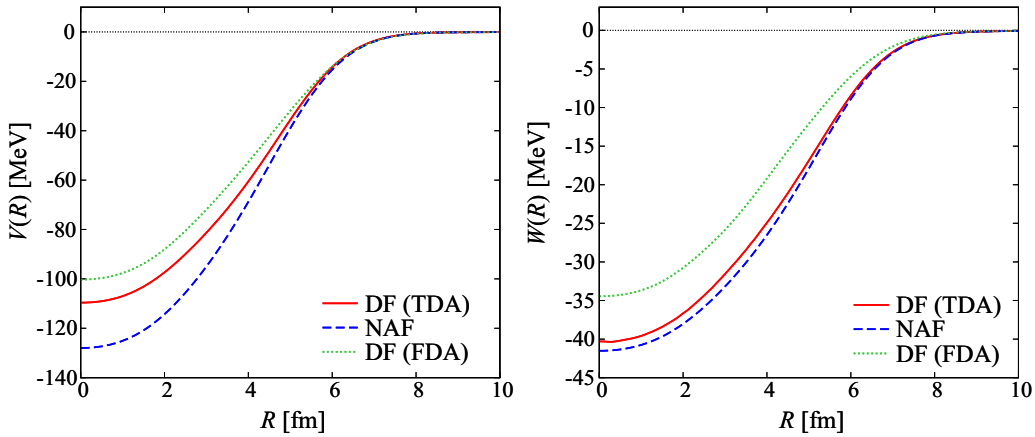

FIG. 5. (Color online) Optical potentials for ^{4}He + ^{58}Ni elastic scattering at $E_{\rm in}/A_{\rm P} = 85$ MeV. See Fig. 4 for the definition of lines.

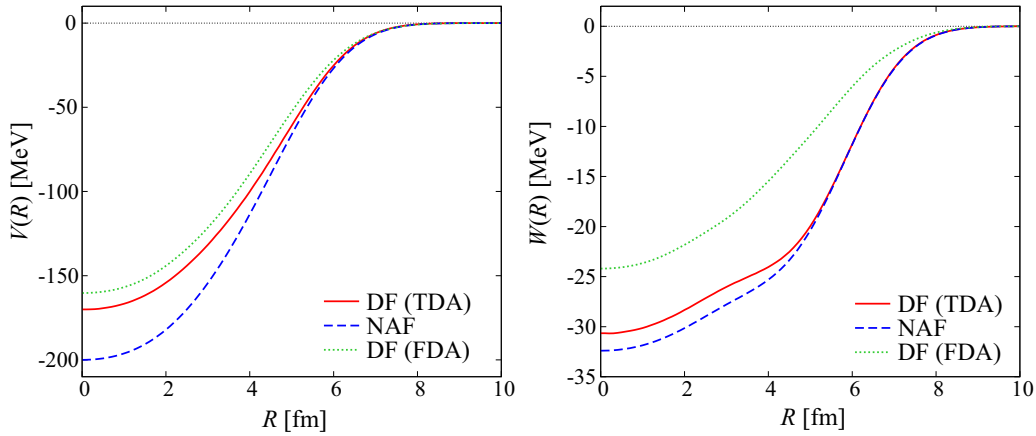

FIG. 6. (Color online) Optical potentials for ^{4}He + ^{58}Ni elastic scattering at $E_{\rm in}/A_{\rm P} = 26$ MeV. See Fig. 4 for the definition of lines.

for $R \lesssim 5$ fm. The deviation does not contribute to $d\sigma/d\Omega$ and $\sigma_{\rm R}$, since the elastic S-matrix elements are quite small for $R \lesssim 5$ fm. This is the reason why the NAF model is good for lower energies. For $E_{\rm in}/A_{\rm P} = 85$ MeV, meanwhile, the NAF potential is largely deviated from the DF-TDA potential for $R \lesssim 5$ fm, whereas the elastic S-matrix elements are small only for $R \lesssim 3$ fm. The NAF model is thus not good for intermediate energies around $E_{\rm in}/A_{\rm P} = 85$ MeV.

Finally, we briefly discuss ^{4}He + ^{208}Pb elastic scattering. Figure 7 shows $d\sigma/d\Omega$ as a function of q for ^{4}He + ^{208}Pb scattering at (a) $E_{\rm in}/A_{\rm P} = 26$–85 MeV and (b) $E_{\rm in}/A_{\rm P} =$ 97–175 MeV. The same statement is possible also for the ^{208}Pb target. Namely, the DF-TDA model yields better agreement with the experimental data [44,47–49] than the DF-FDA model. The NAF model well simulates the DF-TDA model for lower energies around $E_{\rm in}/A_{\rm P} = 30$ MeV and also for higher energies around $E_{\rm in}/A_{\rm P} = 175$ MeV.

IV. SUMMARY

We presented a reliable double-folding model for ^{4}He scattering from heavier targets such as ^{58}Ni and ^{208}Pb in a

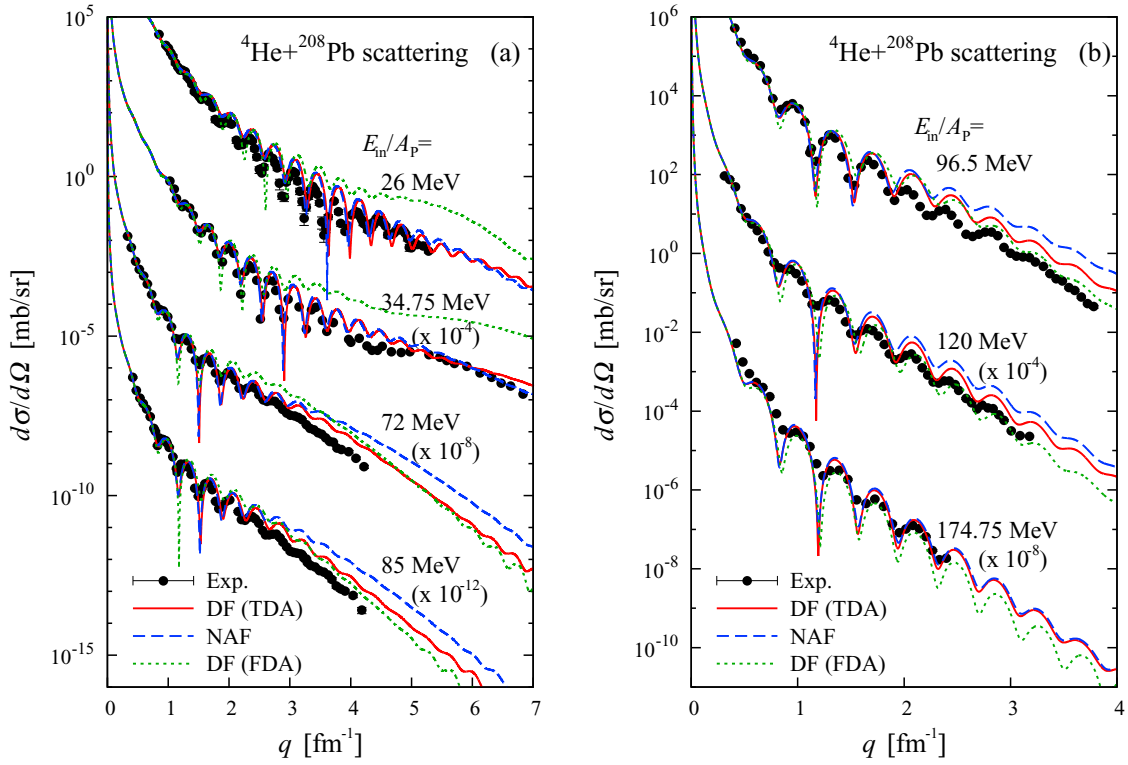

FIG. 7. (Color online) Differential cross sections as a function of transfer momentum q for ^{4}He + ^{208}Pb elastic scattering at (a) $E_{\rm in}/A_{\rm P} =$ 26–85 MeV and (b) $E_{\rm in}/A_{\rm P} = 97$–175 MeV. The cross section at each $E_{\rm in}/A_{\rm P}$ is multiplied by the factor shown in the panel. The solid (dotted) line stands the results of the DF-TDA (DF-FDA) model, whereas the dashed line denotes the results of the NAF model. The experimental data are taken from [44,47–49].

wide range of incident energies from 20 to 200 MeV/nucleon: the Melbourne g-matrix DF model with the target-density approximation (TDA), i.e., the DF-TDA model. The reliability of the DF-TDA model was shown theoretically by using multiple scattering theory and phenomenologically by showing that the model reproduces measured $d\sigma/d\Omega$ and σ_R. The DF-TDA model yields much better agreement with the experimental data than the usual DF model with the frozen-density approximation.

We also investigated the reliability of the NAF model in which the NA potential is folded with the ^{4}He density. This model is quite practical, since we can use the phenomenological NA optical potential instead of the microscopic NA optical potential. The NAF model well simulates the DF-TDA model for lower energies around $E_{in}/A_P = 30$ MeV and also for higher energies around $E_{in}/A_P = 175$ MeV.

The success of the DF-TDA model for ^{4}He scattering comes from the fact that ^{4}He is strongly bound and has no excited state below 20 MeV. Weakly bound nuclei such as d and ^{6}He do not have these properties. This indicates that the DF-TDA and NAF models are not good for explaining the scattering. However, it is well known that the scattering well described by three- and four-body models [1–3]. For a ^{6}He projectile, for example, the scattering is described by the $^4\mathrm{He} + n + n + \mathrm{T}$ four-body model [3] in which the potential between ^{4}He and a target T is obtained by using the double-folding model and the potential between n and T is obtained by using the single-folding model consistently. If the DF-TDA model is applied, it will provide an accurate optical potential for the $^4\mathrm{He} + \mathrm{T}$ subsystem.

ACKNOWLEDGMENTS

This work is supported in part by Grants-in-Aid for Scientific Research (No. 244137 and No. 26400278) from the Japan Society for the Promotion of Science (JSPS).

[1] M. Kamimura, M. Yahiro, Y. Iseri, Y. Sakuragi, H. Kameyama, and M. Kawai, Prog. Theor. Phys. Suppl. **89**, 1 (1986).
[2] N. Austern, Y. Iseri, M. Kamimura, M. Kawai, G. Rawitscher, and M. Yahiro, Phys. Rep. **154**, 125 (1987).
[3] M. Yahiro, K. Ogata, T. Matsumoto, and K. Minomo, Prog. Theor. Exp. Phys. **2012**, 01A206 (2012).
[4] G. Bertsch, J. Borysowicz, H. McManus, and W. G. Love, Nucl. Phys. A **284**, 399 (1977).
[5] J.-P. Jeukenne, A. Lejeune, and C. Mahaux, Phys. Rev. C **16**, 80 (1977); Phys. Rep. **25**, 83 (1976).
[6] F. A. Brieva and J. R. Rook, Nucl. Phys. A **291**, 299 (1977); **291**, 317 (1977); **297**, 206 (1978).
[7] G. R. Satchler and W. G. Love, Phys. Rep. **55**, 183 (1979).
[8] G. R. Satchler, *Direct Nuclear Reactions* (Oxford University Press, New York, 1983).
[9] N. Yamaguchi, S. Nagata, and T. Matsuda, Prog. Theor. Phys. **70**, 459 (1983); **76**, 1289 (1986).
[10] L. Rikus, K. Nakano, and H. V. Von Geramb, Nucl. Phys. A **414**, 413 (1984); L. Rikus and H. V. Von Geramb, *ibid.* **426**, 496 (1984).
[11] K. Amos, P. J. Dortmans, H. V. Von Geramb, S. Karataglidis, and J. Raynal, in *Advances in Nuclear Physics*, edited by J. W. Negele and E. Vogt (Plenum, New York, 2000), Vol. 25, p. 275.
[12] T. Furumoto, Y. Sakuragi, and Y. Yamamoto, Phys. Rev. C **78**, 044610 (2008); **79**, 011601(R) (2009); **80**, 044614 (2009).
[13] S. M. Saliem and W. Haider, J. Phys. G **28**, 1313 (2002).
[14] B. Sinha, Phys. Rep. **20**, 1 (1975); B. Sinha and S. A. Moszkowski, Phys. Lett. B **81**, 289 (1979).
[15] H. F. Arellano, F. A. Brieva, and W. G. Love, Phys. Rev. C **52**, 301 (1995).
[16] D. T. Khoa, W. von Oertzen, H. G. Bohlen, and S. Ohkubo, J. Phys. G **34**, R111 (2007).
[17] T. Furumoto, Y. Sakuragi, and Y. Yamamoto, Phys. Rev. C **82**, 044612 (2010).
[18] T. Sumi *et al.*, Phys. Rev. C **85**, 064613 (2012).
[19] K. Minomo, K. Ogata, M. Kohno, Y. R. Shimizu, and M. Yahiro, J. Phys. G **37**, 085011 (2010).
[20] K. Hagino, T. Takehi, and N. Takigawa, Phys. Rev. C **74**, 037601 (2006).
[21] M. Toyokawa, K. Minomo, and M. Yahiro, Phys. Rev. C **88**, 054602 (2013).
[22] A. J. Koning and J. P. Delaroche, Nucl. Phys. A **713**, 231 (2003).
[23] S. Hama, B. C. Clark, E. D. Cooper, H. S. Sherif, and R. L. Mercer, Phys. Rev. C **41**, 2737 (1990).
[24] E. D. Cooper, S. Hama, B. C. Clark, and R. L. Mercer, Phys. Rev. C **47**, 297 (1993).
[25] C. M. Perey and F. G. Perey, At. Data Nucl. Data Tables **17**, 1 (1976).
[26] K. M. Watson, Phys. Rev. **89**, 575 (1953).
[27] A. K. Kerman, H. McManus, and R. M. Thaler, Ann. Phys. (NY) **8**, 551 (1959).
[28] M. Yahiro, K. Minomo, K. Ogata, and M. Kawai, Prog. Theor. Phys. **120**, 767 (2008).
[29] T. Furumoto and Y. Sakuragi, Phys. Rev. C **74**, 034606 (2006).
[30] K. Minomo, T. Sumi, M. Kimura, K. Ogata, Y. R. Shimizu, and M. Yahiro, Phys. Rev. C **84**, 034602 (2011).
[31] K. Minomo, T. Sumi, M. Kimura, K. Ogata, Y. R. Shimizu, and M. Yahiro, Phys. Rev. Lett. **108**, 052503 (2012).
[32] M. Kimura and H. Horiuchi, Prog. Theor. Phys. **111**, 841 (2004).
[33] M. Kimura, Phys. Rev. C **75**, 041302(R) (2007).
[34] J. F. Berger, M. Girod, and D. Gogny, Comput. Phys. Commun. **63**, 365 (1991).
[35] D. T. Khoa and D. C. Cuong, Phys. Lett. B **660**, 331 (2008).
[36] G. Takeda and K. M. Watson, Phys. Rev. **97**, 1336 (1955).
[37] A. Picklesimer and R. M. Thaler, Phys. Rev. C **23**, 42 (1981).
[38] H. de Vries, C. W. de Jager, and C. de Vries, At. Data Nucl. Data Tables **36**, 495 (1987).
[39] R. P. Singhal, M. W. S. Macauley, and P. K. A. De Witt Huberts, Nucl. Instrum. Methods **148**, 113 (1978).
[40] H. H. Chang, B. W. Ridley, T. H. Braid, T. W. Conlon, E. F. Gibson, and N. S. P. King, Nucl. Phys. A **270**, 413 (1976).
[41] H. Rebel, R. Löhken, G. W. Schweimer, G. Achatz, and G. Hauser, Z. Phys. **256**, 258 (1972).
[42] J. Albiński *et al.*, Nucl. Phys. A **445**, 477 (1985).

[43] Y.-W. Lui, D. H. Youngblood, H. L. Clark, Y. Tokimoto, and B. John, Phys. Rev. C **73**, 014314 (2006).
[44] B. Bonin *et al.*, Nucl. Phys. A **445**, 381 (1985).
[45] B. K. Nayak *et al.*, Phys. Lett. B **637**, 43 (2006).
[46] A. Ingemarsson *et al.*, Nucl. Phys. A **676**, 3 (2000).
[47] G. Hauser, R. Löhken, H. Rebel, G. Schatz, G. W. Schweimer, and J. Specht, Nucl. Phys. A **128**, 81 (1969).
[48] D. A. Goldberg, S. M. Smith, H. G. Pugh, P. G. Roos, and N. S. Wall, Phys. Rev. C **7**, 1938 (1973).
[49] M. Uchida *et al.*, Phys. Rev. C **69**, 051301(R) (2004).